

# 1    **Recent and projected changes in rain-on-snow event characteristics**

## 2    **across Svalbard**

3    Hannah Vickers<sup>1</sup>, Priscilla Mooney<sup>1</sup> and Oskar Landgren<sup>2</sup>

4    <sup>1</sup>NORCE Norwegian Research Centre, Bergen, Norway

5    <sup>2</sup>Norwegian Meteorological Institute, Oslo, Norway

6    *Correspondence to:* Hannah Vickers (havi@norce-research.no)

### 7    **Abstract.**

8    Rain-on-snow (ROS) events in Svalbard are occurring more frequently during the winter season due to rapid and ongoing  
9    climate warming across the Arctic. ROS events have gained increasing attention in recent decades due to their cascading  
10    impacts on the physical environment, and terrestrial and marine ecosystems that are impacted by snowmelt. While the  
11    frequency of ROS events in Svalbard has been well studied and documented, other characteristics of ROS, specifically their  
12    duration, intensity and seasonal timing have received less attention. Such characteristics are equally important to quantify due  
13    to their potential consequences for the winter snowpack and snow-dependent ecosystems. This study addresses this knowledge  
14    gap using the Copernicus Arctic Regional Reanalysis (CARRA) for the present-day analysis and km-scale climate projections  
15    from the HARMONIE Climate (HCLIM) regional model obtained by downscaling the Max Planck Institute for Meteorology  
16    Earth System Model Version 1.2 at Low Resolution. The HCLIM projections cover the near future period of 2030-2070 under  
17    the high emissions scenario SSP5-8.5. For the present climate, the results show significant and positive trends in the mean  
18    duration, intensity and total precipitation of ROS events but these are confined mainly to low-lying areas of Nordaustlandet  
19    and some areas in the east of the archipelago, while no statistically significant trend was found in the southern and western  
20    areas which typically exhibit the largest values in these characteristics. On the other hand, there are significant and positive  
21    trends in ROS frequency across most parts of the archipelago except for the highest lying glaciated areas in northern  
22    Spitsbergen and Nordaustlandet. Analysis of the HCLIM future projections showed that the largest changes relative to present  
23    day conditions in all ROS characteristics are projected to occur over the mountainous and glaciated areas in the north and  
24    northeast of the archipelago, while some low lying western coastal areas are projected to experience a decrease. Moreover,  
25    while ROS has increased most in October and May in the present climate, the future climate simulations project a substantial  
26    increase in ROS events in April, which currently experiences very few, if any, ROS events. This may lead to considerable  
27    changes in snow hydrology. The frequency of ROS is projected to increase most over high elevation and glaciated areas in  
28    October, November, April and May by 2070, but with considerable reductions in low lying areas close to the western and  
29    southern coast as well as across many valleys in central Svalbard in October and May. While km-scale models, such as the

30 model used here, reduces some of the uncertainty in projected changes in ROS through improved representation of important  
31 physical processes, their computational costs prohibit the use of model ensembles to address uncertainty in projected changes.  
32 We partially addressed the uncertainty associated with model parameterisation and internal climate variability by analysing  
33 two coarser-resolution, 11km-scale climate projections under the moderate emissions SSP3-7.0 scenario. Our analysis  
34 indicated that there are areas of Svalbard where the change in all ROS characteristics carries greater uncertainty, as  
35 demonstrated by the opposite direction of change exhibited in the two additional global climate models. On the other hand, all  
36 three model projections showed agreement over the increase in ROS frequency over large parts of the archipelago in the 2050-  
37 2070 period. Further work should include analysing a larger ensemble of climate projections downscaled by several RCMs for  
38 Svalbard to produce a broader range of ROS scenarios, as well as carrying out a more in-depth analysis of the changes in  
39 relative contributions of local vs. remote moisture sources to changing patterns of precipitation, and analysing the hydrological  
40 impacts associated with the changes in ROS characteristics identified in this study.

## 41 **1 Introduction**

42 The Arctic is warming at a rate that is three to four times the global average (Rantanen et al., 2022). This enhanced rate of  
43 warming in the Arctic, known as Arctic Amplification, is stronger in the autumn and winter (Screen and Simmonds, 2010;  
44 Zhang et al., 2021) due to ocean-atmosphere feedbacks, and results in substantial changes to the wintertime climate. Interludes  
45 of winter warming bringing rain, often referred to as rain-on-snow (ROS) events, are becoming increasingly frequent across  
46 the High Arctic Archipelago of Svalbard. These events have attracted increasing research attention during the most recent  
47 decade and as such their spatiotemporal characteristics, meteorological drivers and impacts are becoming better understood  
48 and documented using a wide range of observational approaches (e.g. Bartsch et al., 2023; Vickers et al., 2022; Serreze et al.,  
49 2021 Wickström et al., 2020; Peeters et al., 2019; Forbes et al., 2016). These studies include not only their impacts on the  
50 cryosphere, but also on terrestrial and marine/coastal ecosystems as well as society. A significant consequence of ROS events  
51 is the formation of ground ice as rain percolates through the snowpack to the ground-snow interface and refreezes. This presents  
52 a significant barrier to winter forage for reindeer populations in Finnmark and Svalbard and has in some extreme cases resulted  
53 in starvation and large die-offs (e.g., Hansen et al., 2014) as well as adaptations to foraging habits (Pedersen et al., 2021). The  
54 impact of ROS events on the snowpack is largely dependent on the characteristics of a ROS event, such as the total precipitation  
55 and duration, and thus the intensity - as well as the initial properties of the snowpack itself. Snow depth and snowpack  
56 stratigraphy is an important factor which determines how rain percolates through the snowpack and consequently, if ground  
57 ice forms following a ROS event (Peeters et al., 2019) and how surface runoff and hydrology is affected (e.g., Würzer et al.,  
58 2016). Indeed, if a ROS event is intense enough, and the snowpack is thin enough, complete ablation of the snow cover may  
59 occur, removing the wintertime insulation of permafrost as well as increasing the availability of forage to reindeer. Therefore,  
60 the timing and seasonality of ROS events is also an important factor, as this dictates the initial thickness of the snowpack being  
61 impacted.

62 To understand which areas are most vulnerable to ROS impacts at present and in the future, reliable datasets describing the  
63 spatial and temporal variations in ROS are crucial. Recent studies of ROS climatology in Svalbard have exploited Synthetic  
64 Aperture Radar (SAR) remote sensing, due to its sensitivity to liquid water in the snowpack (Vickers et al., 2022). This dataset  
65 was compared to ROS events detected using snow models and atmospheric reanalysis, and good agreement with the SAR  
66 dataset was obtained once the models and reanalysis datasets had been calibrated against ground observations recorded at three  
67 sites across Spitsbergen (Ny Ålesund, Longyearbyen and Hornsund). However, it was shown that different temperature  
68 thresholds were required to produce the best accuracy of ROS detection with respect to the ground observations (Vickers et  
69 al., 2024). Specifically, it was found that gridded atmospheric reanalyses provided by the Copernicus Arctic Regional  
70 Reanalysis (CARRA) dataset was able to capture the frequency of ROS events very accurately when evaluated against ground  
71 observations. Until now most ROS studies of Svalbard have concentrated on documenting ROS frequency, but little attention  
72 has been paid to their duration, intensity, and timing. Earlier analyses of downscaled global climate model (GCM) simulations  
73 have highlighted a potential threefold increase in mild weather days during the winter (October-April) season by 2100, where  
74 precipitation falls on days with temperature above freezing point (Isaksen et al., 2017) while others note an increase exceeding  
75 20% in winter rainfall projected at Longyearbyen airport (Førland et al., 2011) with greatest changes expected in the north and  
76 northeast of the archipelago. As climate warming continues to change the wintertime climate in Svalbard, it is crucial to  
77 quantify how ROS characteristics are influenced by changes in climate, as changes in ROS characteristics will also to a large  
78 degree determine the severity of their impact on snowpack stratigraphy and properties. Moreover, it is of equal importance to  
79 advance our understanding of how these characteristics are likely to change in the coming decades, such that measures can be  
80 planned that will minimise the impacts of ROS on nature and society.

81 Determining possible future changes to ROS climatology across Svalbard has become feasible due to recent advances in  
82 climate modelling and high-performance computing that allow climate models to run at convection-permitting (hereafter, km)  
83 scales. These scales are important for Svalbard as its climate has a large spatial variability arising from its complex topography,  
84 coastlines, fjords, glaciers and surrounding sea ice (Hanssen-Bauer et al. 2019). The benefits of such km-scale climate  
85 projections have been demonstrated already by numerous studies (Mooney et al. 2020; Køltzow et al. 2019; Prein et al. 2015).  
86 Rain-on-snow studies benefit further from these scales as climate models at these resolutions better resolve convective  
87 processes and the important separation of precipitation into rain and snow in km-scale models is physically based as opposed  
88 to the temperature-based approaches used in coarser resolution models (Mooney and Li, 2021). Specifically for Svalbard,  
89 Landgren et al. (2025) produced 2.5 km simulations using the HCLIM-AROME regional climate model (RCM) with input  
90 from the global Earth System Model MPI-ESM1-2-LR under the future scenario SSP5-8.5 (from now on HCLIM-MPI). The  
91 fine resolution of the HCLIM-MPI simulations allows a much-improved representation of the climate of the valleys and  
92 mountains on Svalbard.

93 The CARRA dataset now spans more than 30 years, providing an ideal opportunity to exploit the full time series to document  
94 changes in the characteristics of ROS since 1991. We have derived parameters that include their timing/seasonality, duration,  
95 total precipitation, and intensity, as well as frequency. In addition to studying the spatial variations in these parameters, we

96 also quantify trends in these characteristics over climate-relevant timescales (1991-2023). Lastly, we use high resolution  
97 climate projections from one global climate model downscaled with the HCLIM-AROME RCM to firstly estimate how well  
98 these specific characteristics are represented in the present climate, by comparing the results to those obtained with CARRA  
99 and how they can be expected to change under a warming climate until 2070.

## 100 **2 Methods and Datasets**

### 101 **2.1 Study area**

102 The Svalbard archipelago is located in the North Atlantic Ocean, spanning latitudes between 74 and 81°N and comprises five  
103 main islands, with Spitsbergen being the largest island (Fig.1). Wintertime sea ice is found just north and north-east of  
104 Svalbard, while to the west of the archipelago is the West Spitsbergen Current. The climate of Svalbard is therefore heavily  
105 affected by the location of the sea ice edge, contributing to a strong a southwest-northeast gradient, with milder coastal climates  
106 in the west and south, and cold inland climate influenced by sea ice presence and variability in the north and east (Day et al.,  
107 2012). Annual precipitation at Longyearbyen airport, in the central part of Svalbard is low, and ranges from 121.8mm (2021)  
108 to 310mm (2016), while Ny Ålesund in the northwest part of Svalbard, experiences a substantially wetter climate with annual  
109 precipitation ranging from 205mm (2019) to 749mm (2018). The occurrence of wintertime ROS events is reflected by the  
110 climatic gradient, with highest frequency in the south and west and very few events per winter in the north and east (e.g.,  
111 Wickström et al., 2020; Vickers et al., 2022, 2024).



**Figure 1: Overview of the Svalbard archipelago, showing the main islands (Spitsbergen, Nordaustlandet, Edgeøya, Barentsøya). Bjørnøya lies farthest south and is not shown (source: <https://toposvalbard.npolar.no/> courtesy of the Norwegian Polar Institute).**

## 2.2 CARRA dataset

In this study we use data from the East domain of the Copernicus Arctic Regional Reanalysis (CARRA) dataset, which covers all of Svalbard and its surrounding waters. CARRA provides 3-hourly reanalyses and short-term hourly forecasts of atmospheric and surface meteorological variables at 2.5 km resolution (Schyberg et al., 2020). Earlier evaluations of CARRA have already demonstrated its added value compared to other reanalysis datasets for Svalbard (Køltzow et al., 2022). Following the approach outlined by Vickers et al. (2024), we use the 2m air temperature and snow water equivalent (SWE) reanalyses at 3-hourly resolution and averaged the data to daily values. Forecasted precipitation data at lead times of +6 and +30 hours with initial time 00UT were obtained and the difference was used to calculate the 24-hour accumulated precipitation values from 0600 UTC to 0600 UTC the following day. CARRA data were obtained from 1991 to 2023 to analyse trends for the present-day climate, while only a part of the dataset overlapping with the historical period of the HCLIM simulations was used for model evaluation (2000-2020). Based on the calibration approach described in the earlier study by Vickers et al., 2024, a rain-on-snow *day* was detected when the daily mean 2m temperature was  $>-0.5^{\circ}\text{C}$ , daily precipitation was  $>1\text{mm}$  and SWE was  $>2\text{mm}$ , since these thresholds produced the highest accuracy of ROS day detection when evaluated against in-situ observations.

### 2.3 HCLIM climate model data

This dataset consists of km-scale climate simulations of Svalbard covering the period 1991-2070 and is detailed in Landgren et al. (2025). The data was produced by dynamically downscaling the Max Planck Institute for Meteorology Earth System Model Version 1.2 at Low Resolution (MPI-ESM1-2-LR, Gutjahr et al., 2019) under SSP5-8.5 with the HARMONIE Climate (HCLIM, Belušić et al. 2020, Wang 2024) cycle 43 regional climate model to 2.5 km horizontal grid spacing using nonhydrostatic convection-permitting HARMONIE-AROME atmospheric physics.

For evaluation of present climate conditions, the dataset also consists of a dynamical downscaling of the 5th generation ECMWF Reanalysis (ERA5, Hersbach et al. 2020) with HCLIM for the same domain and resolution but only covering the period 2000-2020. The HCLIM configuration includes the SURFEX land-surface model with ISBA Explicit Snow scheme. More details and evaluation of the 2.5 km simulations and their evaluation over Svalbard are available in Landgren et al. (2025). From here on the HCLIM simulations produced by downscaling the ERA5 Reanalysis data will be referred to as HCLIM-ERA5 and the data produced by downscaling MPI-ESM1-2-LR will be referred to as HCLIM-MPI for clarity.

To identify ROS days in the HCLIM-ERA5 simulations for comparison with the CARRA results for the present climate (2000-2020), we applied the same thresholds as was used for the CARRA dataset, to the variables *pr*, *tas* and *snd*, where *pr* is the accumulated precipitation, which includes both solid and liquid precipitation, *tas* is the 2m air temperature and *snd* is the snow depth water equivalent. All variables are available at 3-hourly intervals, but for the purpose of producing comparable results to CARRA, we have produced daily mean values for the 2m air temperature and snow depth water equivalent variables, and a total daily precipitation estimate by taking the difference between the maximum values of the accumulated precipitation for the following day and the current day. In addition, a *prrain* (accumulated rain) variable was also made available from the RCM simulation to assess the impacts of different approaches for separating rain and snow on the results. The *prrain* variable is derived from the microphysical scheme of the RCM and uses a physics-based approach to separate snow and rain. This contrasts with the approach used in this study which separates rain from snow in the precipitation variables using a temperature threshold-based approach. To detect ROS using *prrain*, we applied the same daily precipitation threshold as we used for the CARRA total daily precipitation (1 mm) and to the snow depth water equivalent (2 mm). We have included the analysis of the ROS characteristics in the present and future climate using the *prrain* variable in the Appendix (Fig.A2 to A5).

### 2.4 Definition of ROS event characteristics

For the purposes of this study, a rain-on-snow event is defined as consecutive rain-on-snow days where the criteria for detection were met. By using this definition, a rain-on-snow *event* can be characterised by its duration, which in turn determines the total precipitation as rain that fell during the event and thereby the average intensity of the event, given by the total precipitation divided by the duration. ROS events are detected in the period 1 October to 31 May *for each winter season*, which includes the shoulder seasons with onset and disappearance of snow cover and the mean values of ROS duration, total precipitation, and intensity are calculated for the time series. The number of ROS events are also recorded for each month of the winter

season to identify spatial variations and trends in their seasonality. Linear regression is performed on the time series to obtain annual trends using the slope of the regression line, and multiplied by ten to obtain the decadal trends, which are presented in section 3. We used the p-value returned by the `scipy.stats.linregress` function to determine if the trend was statistically significant or not ( $p < 0.05$ ).

## 3 Results

### 3.1 Present day climatology and trends in ROS

In Fig. 2 the trend in each ROS characteristic is shown for the full CARRA period (1991-2023) for (a) frequency, (b) duration, (c) total precipitation, and (d) intensity, while the climatological average of each characteristic is shown in Figure 2(e) to (h) for the overlapping period of the CARRA and HCLIM-ERA5 dataset (2000-2020) while the in. For all ROS variables there is a clear southwest-northeast gradient, with typically highest values of ROS frequency, duration, intensity and total precipitation found in the southern and western parts of the archipelago, while the lowest values are found in the more glaciated northern and northeastern areas. While the mean values of each ROS characteristic displayed in Fig.2 (e) to (h) show the overall climatology across the archipelago, there is a large degree of interannual variability as well as geographic variability. This can be seen in the time series of each ROS characteristic shown in Figure A1 for four arbitrary sites chosen for their contrasting locations; Hornsundneset, located at the coast in southwest Spitsbergen; Reindalen, in Nordenskiöld Land; Engelsbukta, just south of Ny Ålesund on the Brøgger peninsula in northwest Spitsbergen, and Åsgårdfonna, a high elevation glaciated region in the north of Spitsbergen. Addressing first the significant trends since 1991 (grid cells where  $p < 0.05$  only), it is evident that significant and positive trends are found predominantly across eastern and north-eastern areas of the archipelago in all characteristics. For the ROS frequency (Fig. 2(a)), significant and positive trends are much more widespread than for the other ROS characteristics, and are also found in southern, western and central parts of the archipelago, as well as in the coastal parts of the northeast and across Edgeøya. Across Nordaustlandet, increases of up to 1 event per winter per decade are found around the coastal areas which include both land and glaciated parts. On Spitsbergen, positive trends of up to 2 to 2.5 events per winter per decade are occurring across Nordenskiöld Land as well as the southern parts of Spitsbergen and some areas in the northwest. ROS frequency is also increasing over most of Edgeøya. Examining the trends in the duration, total precipitation, and mean intensity of ROS events, there are also positive and significant trends, but the geographic variations are somewhat different compared to the trends in ROS frequency. For ROS duration (Fig. 2(b)), significant and positive trends are mainly confined to low-lying valley areas across eastern parts of Nordenskiöld Land and northern Spitsbergen but on Nordaustlandet positive trends are exhibited around the entire coast of the island, and in general the decadal trends are also greatest here, with increases of up to 0.5 days per event. Related to the positive trend in ROS duration is a positive trend in the total precipitation (Fig. 2(c)) and intensity (Fig. 2(d)), which is exhibited across the same areas on Nordaustlandet and eastern parts of Spitsbergen. Typical trends in these areas are of the order 2 to 4 mm per event per decade for total precipitation and around 1

191 to 2.5 mm/day per decade in ROS intensity. Somewhat larger increases in total precipitation of 4-5mm per event (per decade)  
192 are found on Edgeøya and Barentsøya.

193 Figure 2(i) to (l) shows the climatological means of the ROS frequency, duration, total precipitation and intensity obtained  
194 using the HCLIM-ERA5 downscaled to 2.5km. The differences between these means and the CARRA mean for the  
195 corresponding variable are shown in panels (m) to (p). The differences are calculated as HCLIM minus CARRA. Comparing  
196 the climatological averages of the characteristics obtained using CARRA (Fig. 2 (e) to (h)) and the 2.5km HCLIM-ERA5 (Fig.  
197 2(i) to (l)) for the present climate, the geographical variations are reproduced reasonably well by the HCLIM-ERA5 dataset  
198 even though the absolute values for all characteristics are lower with respect to the CARRA output for the ROS frequency and  
199 duration. The difference is typically of the order of 1 to 2 events per winter and 0.5 to 0.75 days per event respectively, with  
200 CARRA showing higher values over most of the archipelago, except for across the larger glaciated areas over Nordaustlandet  
201 where HCLIM-ERA5 dataset tends to show slightly more ROS events than the CARRA simulations.



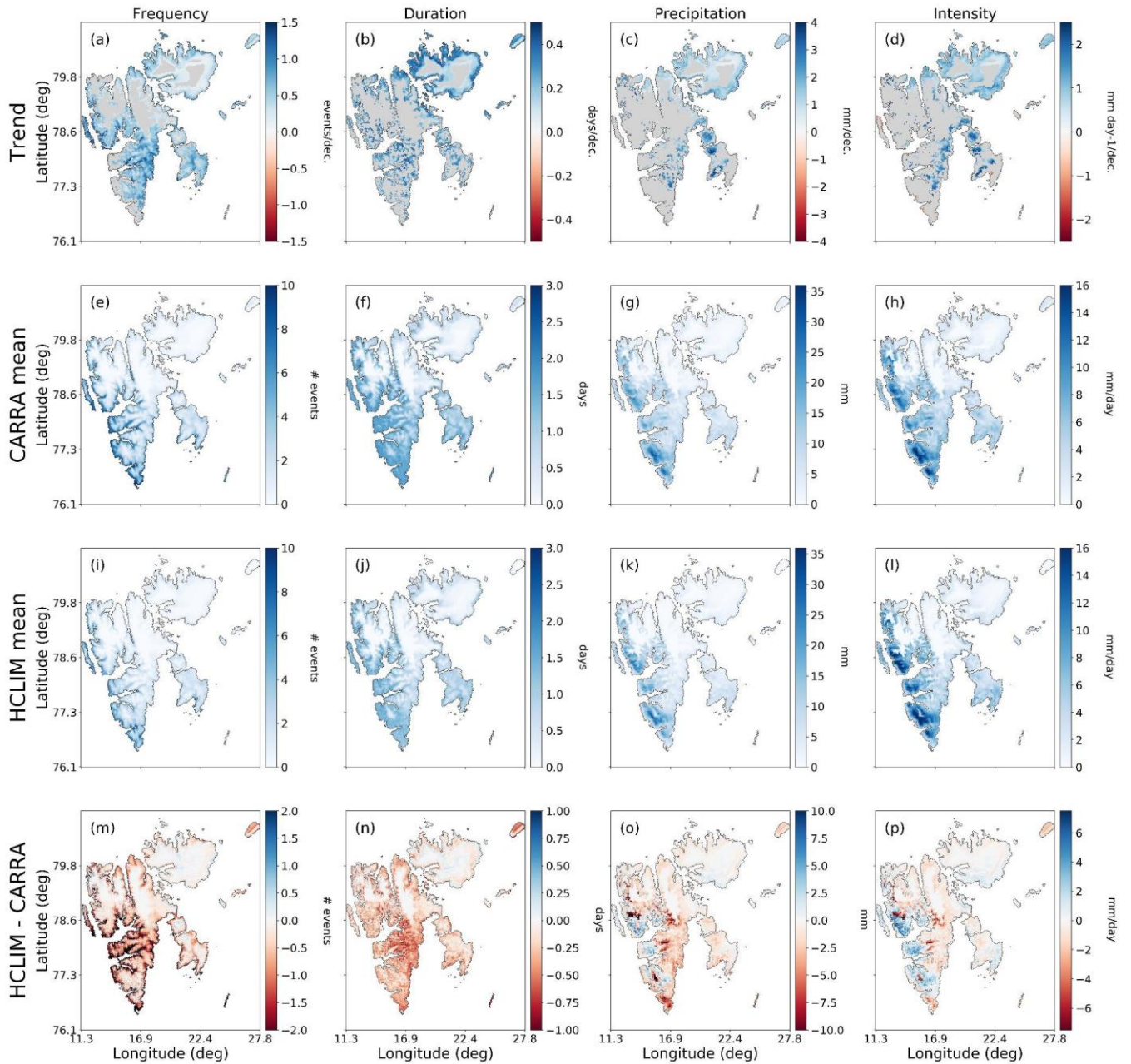


**Figure 2: Present day trends derived from the CARRA dataset (a to d) and climatology of ROS frequency, duration, total precipitation per event, and mean intensity for 2000-2020 (e) to (h). Trends are obtained for the entire CARRA period (1991-2023). ROS climatology for 2000-2020 obtained with HCLIM-ERA5 at 2.5km resolution (i to l) and the differences between HCLIM-ERA5 and CARRA (m to p).**

For ROS frequency, both CARRA and HCLIM-ERA5 show that there is a southwest-northeast gradient, with ROS occurring most frequently in the southwest and western coastal areas of Spitsbergen and decreasing across inland areas. However, while ROS are at present occurring less frequently across eastern and inland areas of the archipelago, one may note that it is these

210 areas where ROS have been increasing in frequency during the past 30 years (Fig. 2 (a)). The same climatic gradients are  
 211 exhibited by the averages of ROS duration, total precipitation, and intensity. However, the contrast between western and  
 212 southwestern coastal areas and inland areas of Spitsbergen is not so prominent for ROS duration as it is for total precipitation  
 213 and intensity. The mean duration of ROS events is of the order of 1-2 days across the southern, central, and north-western parts  
 214 of Spitsbergen, with an overall agreement in CARRA and HCLIM-ERA5. However, comparing the mean ROS total  
 215 precipitation and intensity, HCLIM-ERA5 tends to estimate higher total precipitation along the western coast compared to  
 216 CARRA, even though the mean event duration in these areas is only marginally lower, leading to an overall higher event  
 217 intensity in the HCLIM-ERA5 dataset in these western regions. The lower intensity in these regions in the CARRA dataset is  
 218 likely the result of slightly longer ROS durations estimated by CARRA, while total precipitation is also overall lower than  
 219 HCLIM-ERA5 in these areas. On the other hand, CARRA tends to estimate higher total precipitation across the more eastern,  
 220 southern and inland parts of the archipelago, as well as in parts of the north. However, the greatest differences between the  
 221 datasets for the mean total precipitation are typically only of the order 5 to 7 mm per ROS event.

222 Figure 3 decomposes the trend in ROS frequency by month using the CARRA dataset from 1991-2023. Only significant trends  
 223 ( $p < 0.05$ ) are shown, while non-significant trends are indicated by the grey shading. It is striking to note that ROS frequency  
 224 has increased significantly in predominantly three months of the winter season; mid to late autumn (October - November) and  
 225 spring (May). Less widespread and weaker trends are also observed in February. Moreover, the geographical distribution of  
 226 the significant trends is different and contrasting for these months; in October, positive trends in ROS frequency are  
 227 predominantly found around the coastal areas of Nordaustlandet, eastern and southern Spitsbergen and Edgeøya, areas  
 228 typically associated with a colder inland climate, as well as some higher elevation parts of the northwest while in February the  
 229 significant and positive trends are found only along the low lying parts of the western coast of Spitsbergen and some parts of  
 230 southern Spitsbergen, typically associated with a milder maritime climate. In May, significant and positive trends are found  
 231 over most of Nordenskiöld Land, northwest and southern Spitsbergen as well as parts of Edgeøya and Barentsøya. The trends  
 232 exhibited in ROS frequency exhibited in Fig. 3 thus originate mainly from changes in ROS frequency during October,  
 233 November and May, while ROS frequency during all other months of the winter have not changed significantly since 1991.

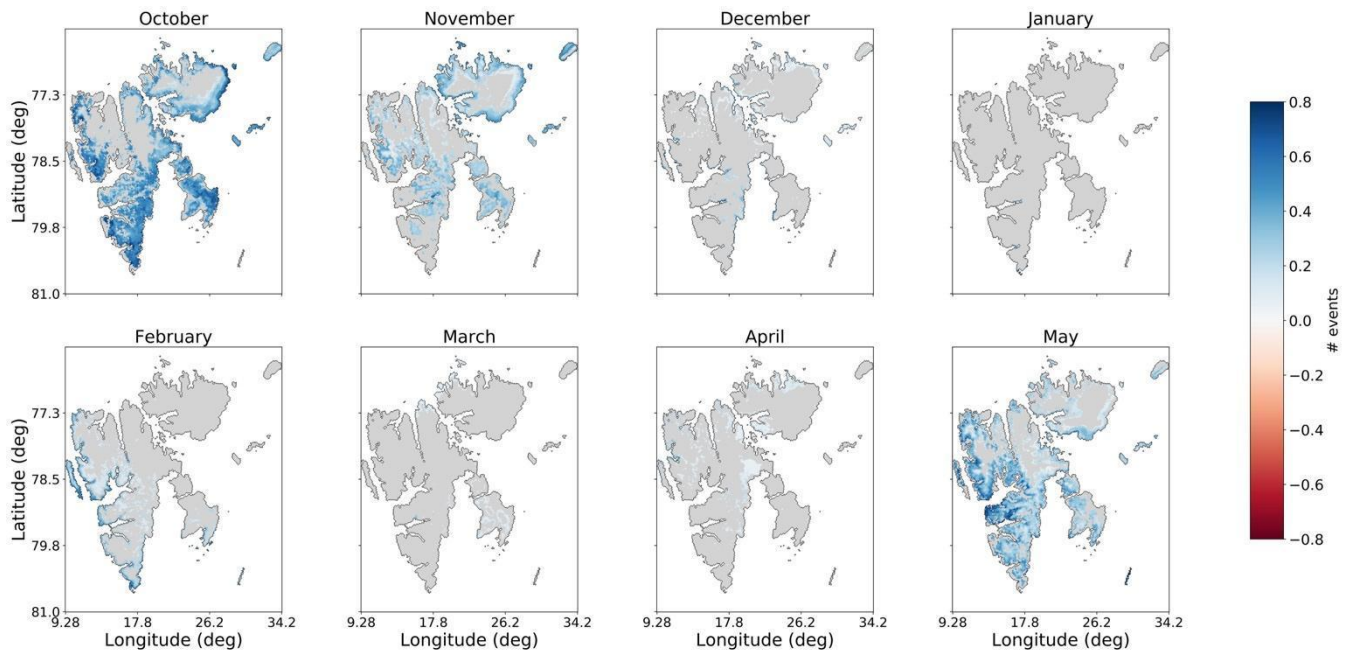


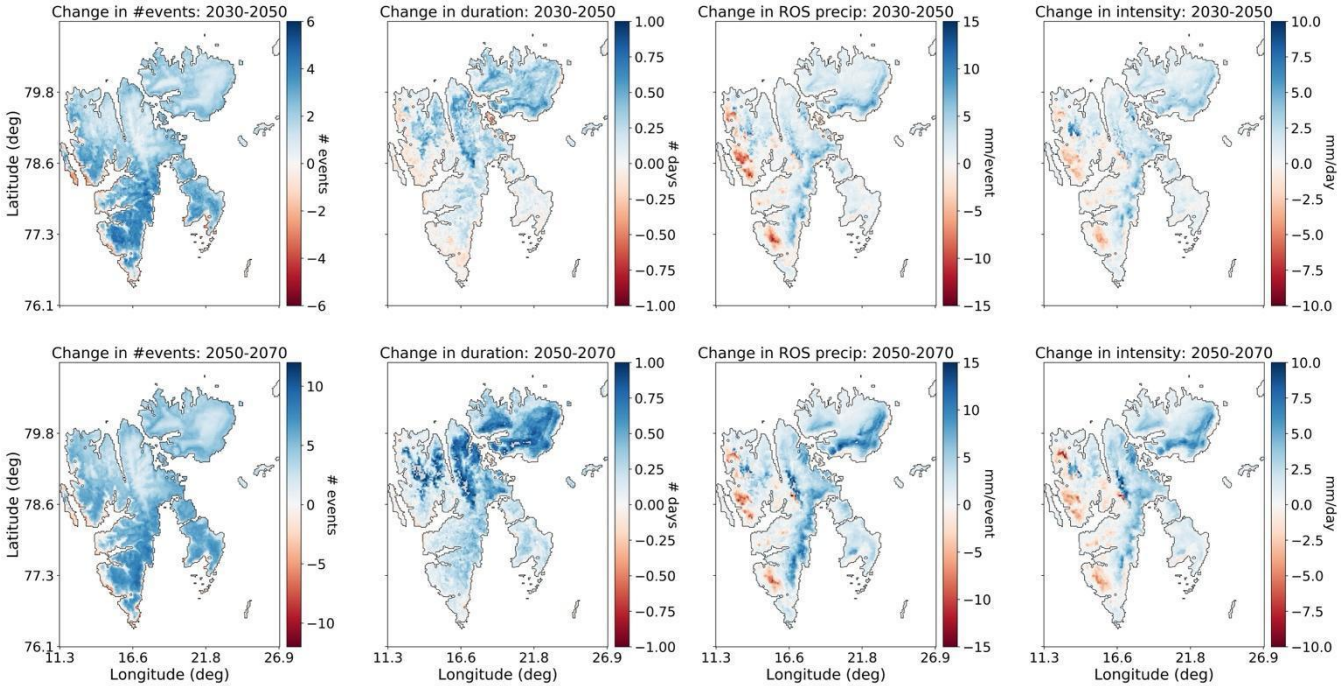
**Figure 3: Decadal trend in number of events per month from October to May for the 1991-2023 CARRA period. Only significant trends ( $p < 0.05$ ) are shown while grey areas correspond to areas with non-significant trends.**

In Sect. 3.2 we examined the projected changes in ROS during the next four decades under a high emissions scenario, obtained using the HCLIM-downscaled climate projections from the MPI global climate model.

### 3.2 Projected future changes in ROS characteristics

Figure 4 shows the projected change in the mean number of ROS events, the mean duration, total precipitation, and intensity in the 2030-2050 and 2050-2070 periods from the HCLIM-MPI dataset, compared to the mean for the historical period (2000-2020). In terms of the absolute changes, Fig.4 shows that for both the future periods examined, 2030-2050 and 2050-2070, HCLIM-MPI projects an increase in frequency of ROS events that is greatest over the areas where significant and positive trends in frequency were identified in Fig.2. That is to say, the areas that are projected to have the greatest increase in number of ROS events are across the eastern and southern parts of Spitsbergen, as well as across Edgeøya and Barentsøya. Northern parts of Spitsbergen and Nordaustlandet are also projected to experience increases in ROS frequency, but to a lesser degree. At the same time, the lowest lying coastal areas in western Spitsbergen are projected to experience a decrease in ROS frequency in the two future periods. The change in mean number of events for the 2050-2070 period could be twice as great as for the 2030-2050 period, as indicated by the different colour scales used in Fig.4. The geographical variation in change in ROS events is somewhat different to the geographical variations in ROS frequency for the present climate, where ROS are currently dominant in the western part of Spitsbergen, but exhibits similarities to the geographical variations in significant trends since 1991 (Fig. 2). Figure 4 shows that the mean duration of ROS events is projected to increase by up to 1 day in the future

253 scenario, with the largest increases in the northern and north-eastern parts of the archipelago, as well as weaker increases in  
 254 mean ROS duration across eastern parts of Nordenskiöld Land and Edgeøya. Thus, ROS duration is projected to increase most  
 255 over glaciated and mountainous areas in the northern part of the archipelago, where there are very few ROS events in the  
 256 present climate (Fig. 2). This could be due to an overall increase in wintertime temperatures, leading to a greater probability  
 257 of days above freezing with precipitation than in the present climate. However, these areas with the greatest increase in mean  
 258 ROS event duration currently have a mean duration between 0 to 0.5 days in the present climate, indicating that there are at  
 259 present only isolated ROS events that do not occur every winter. The mean projected increase in ROS event duration is typically  
 260 only of the order of 1 day (at most) by the 2050-2070 period over these areas, while the mean increase in number of events in  
 261 the areas that exhibit greatest increase in duration is of the order of 2-3 events for the same period, indicating that the ROS  
 262 events that do occur may be single-day events. At the same time there are projected decreases in the mean duration, total  
 263 precipitation and mean intensity of events across the western coastal parts of Spitsbergen in both future periods examined,  
 264 even though there are projected to be increases in ROS frequency in these areas. For the changes in ROS total precipitation  
 265 and intensity, several specific regions stand out as having the largest projected increases; the east coast of Spitsbergen (up to  
 266 15 mm per event) and across the southern and eastern coastal areas of Nordaustlandet. Notably, the change in total precipitation  
 267 and intensity by 2050-2070 (with respect to 2000-2020) is only slightly greater than the changes in 2030-2050. This differs  
 268 from the ROS frequency and duration, where the increases are projected to be twice as great and over large areas in the 2050-  
 269 2070 period compared to 2030-2050.

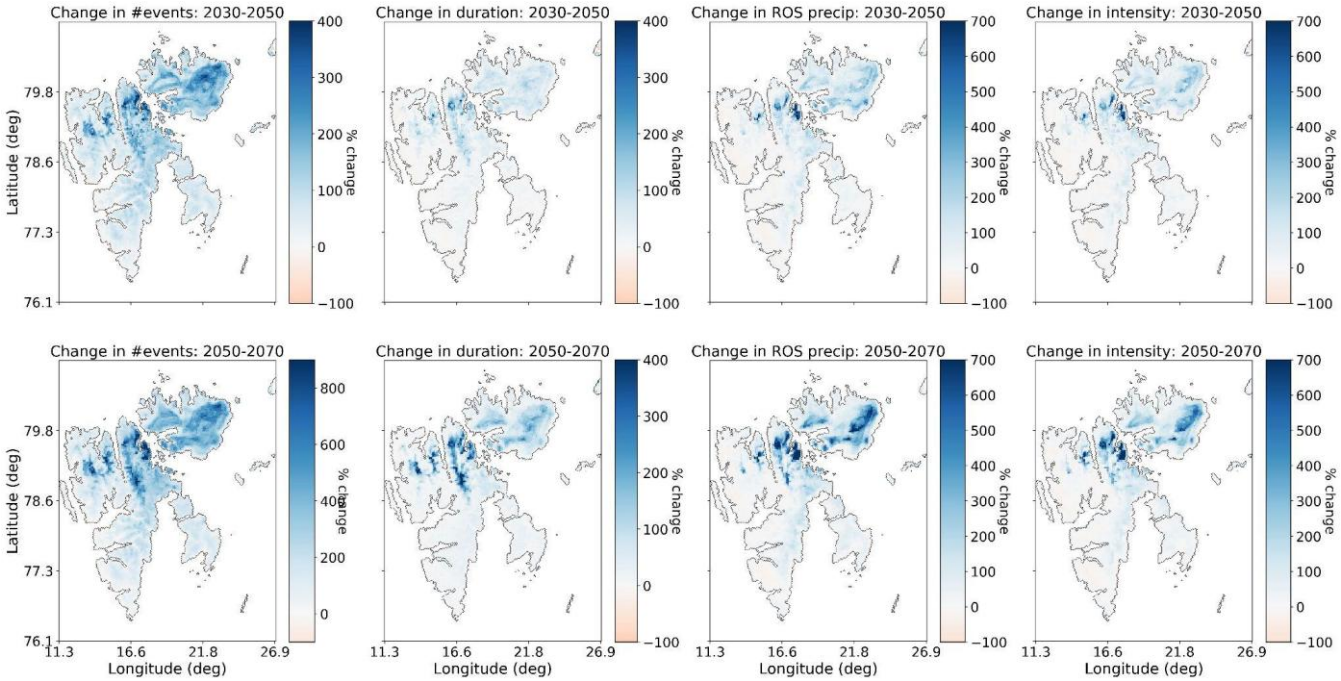


270  
 271 **Figure 4: Change in ROS frequency, duration, total precipitation, and mean intensity using the HCLIM-MPI dataset for 2030-2050**  
 272 **(upper row) and 2050-2070 (lower row) relative to the 2000-2020 averages.**



273  
274  
275  
276  
277  
278  
279  
280  
281  
282  
283  
284

Figure 5 also shows the projected changes in the four ROS characteristics but expressed as the percentage change relative to the 2000-2020 mean as opposed to the absolute values. This approach illustrates the areas that could experience the most dramatic changes in the ROS characteristics with respect to the present-day climatology. The glaciated and mountainous regions in northern Spitsbergen and especially across Nordaustlandet are projected to undergo the greatest change relative to the 2000-2020 average. While the percentage changes in ROS frequency are very large for areas projected to experience the greatest change (~300% in 2030-2050, ~700-800% in 2050-2070), it should be recalled that the mean frequency, duration, total precipitation and intensity of ROS events across these areas are at present very low; thus, even a change producing on average one single-day ROS event per winter results in change of several hundred percent relative to the present-day values. Nevertheless, such considerable relative changes over glaciated areas may have considerable impacts on hydrology, which could subsequently have consequences for fjord and marine ecosystems due to increased freshwater runoff during the wintertime. This will be further discussed in Sect. 4.



285

286 **Figure 5: Change in ROS frequency, duration, total precipitation, and mean intensity using the HCLIM-MPI dataset for 2030-2050**  
287 **(upper row) and 2050-2070 (lower row) expressed as a percentage of the 2000-2020 averages.**

288 In Fig. 6 the projected changes of ROS frequency are shown for each month of the winter period (October-May). For the earlier  
289 2030-2050 period, the greatest increase in the number of ROS events is projected to occur in October across eastern parts of  
290 Spitsbergen, as well as across eastern parts of Nordaustlandet and on Edgeøya. Noticeable decreases of up to 2 events per  
291 winter are projected along the entire western coast of Spitsbergen in October. A similar pattern of change is also projected for  
292 November in the 2030-2050. Meanwhile, increases in ROS frequency during May are projected in the western and southern

parts of Spitsbergen. Smaller increases (0.5-1 events per winter) in the mean ROS frequency are projected to take place in January and February, but confined to the western, central, and southern parts of Spitsbergen. By 2050-2070 the situation changes quite dramatically. While both increases and decreases in the mean ROS frequency may continue to occur in October, November and May across the same areas as during the 2030-2050 period, increases in ROS frequency ( $>1.5$  events per winter) are projected to occur in April, and these changes are present across large parts of the entire archipelago. Only some glaciated parts of northern Spitsbergen and Nordaustlandet are not projected to have such great increases in ROS frequency during April in the 2050-2070 period. Furthermore, changes in ROS frequency of comparable magnitude could also take place during January, a month that has until now not experienced significant changes in ROS frequency (Fig. 2). In Fig. 6 it can also be seen that there are projected to be weak decreases in the mean number of ROS events in some areas of the northern and eastern Spitsbergen in December, and across western and southern areas during March for the 2030-2050 period. However, in the later future period (2050-2070) these same areas exhibit increases with respect to 2000-2020.

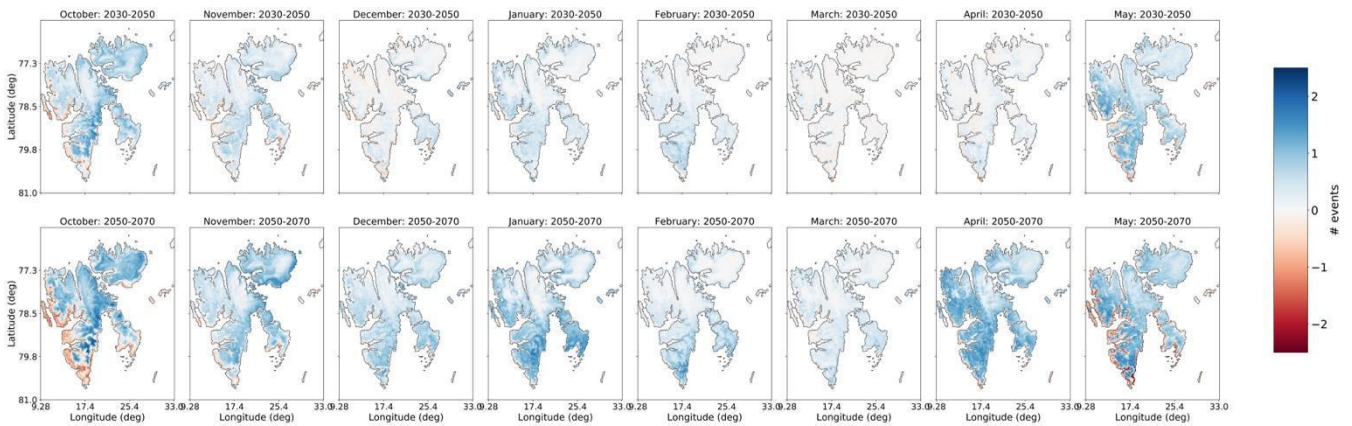
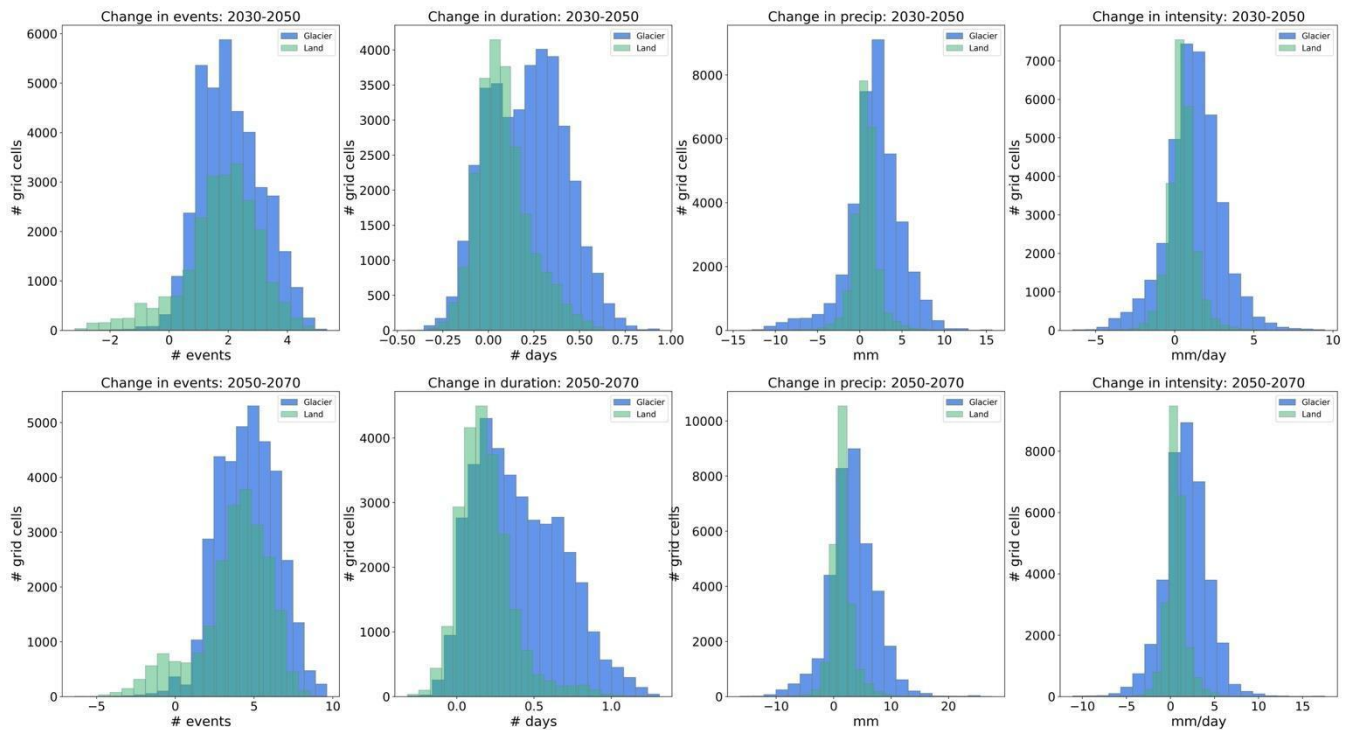


**Figure 6: Changes in ROS frequency by month from October to May using the HCLIM-MPI dataset, for 2030-2050 (upper row) and 2050-2070 relative to the reference period 2000-2020.**

Figure 7 shows the spatial distribution of the absolute change in ROS frequency, duration, total precipitation and intensity for land and glaciers. For the ROS frequency in the near-future period (2030-2050), both land and glacier areas exhibit a change ranging from -2 to +4 events per winter on average compared to 2000-2020, while for the latter period (2050-2070) this change is clearly almost doubled with a range from -4 to +10 events. For glaciers there are no areas experiencing a reduction in frequency for the two periods, while there are some areas with a decrease in frequency across land areas. There is also a clear positive shift in the distribution of change in ROS duration for glaciers compared to the change in mean ROS duration for land areas, which is most prominent for the 2053-2050 period. While the peaks of the mean duration distributions lie at roughly +0.05 and +0.3 days for land and glaciers respectively in 2030-2050, the peaks lie at +0.2 days for both land and glaciers in the 2050-2070 period, but with the distribution for glaciers skewed such that the majority of the glaciated areas exhibit increased ROS duration of up to +1.2 days in the later 2050-2070 period. Likewise, there is a shift in the peak of the distribution of the projected ROS total precipitation over glaciers with an increase of +2mm in 2030-2050 relative to the 2000-2020 period and +4mm increase by 2050-2070. For land areas, the overall change in the mean total precipitation has a peak at +1mm and

319 +2mm for each future period respectively. For ROS intensity, the mean change lies at approximately +2mm/day in both future  
 320 periods and the distribution of changes for land and glaciers overlap. While the change in ROS frequency over glaciers is  
 321 mostly positive, it can be seen that there are both positive and negative changes in the ROS duration, intensity and total  
 322 precipitation for both land and glaciers.

323



324

325 **Figure 7: Spatial distribution of change in ROS frequency, duration, total precipitation and mean intensity for 2030-2050 (upper**  
 326 **row) and 2050-2070 (lower row) shown for land and glaciers separately.**

## 327 4 Discussion

328 This study has utilized a 32-year time series of an atmospheric reanalysis and a 70-year time series of a km-scale climate  
 329 simulation for Svalbard to (i) study how four characteristics of ROS events have changed in the most recent three decades  
 330 from 1991 to 2022, and (ii) how they may change in the forthcoming decades, specifically, 2030-2050 and 2050-2070, as  
 331 represented by one km-scale regional climate model simulation under a high greenhouse gas emissions scenario.

332

#### 4.1 Analysis of ROS characteristics in the present climate

Statistically significant and positive trends in all parameters were found predominantly in the lower-lying outskirts of Nordaustlandet in the north-east of the archipelago, and across Edgeøya in the southeast, while significant increases in frequency were also found across the eastern areas of Spitsbergen. No significant trends in mean ROS duration, intensity and total precipitation were found in the western parts of Nordenskiöld Land and southwest Spitsbergen, where ROS frequency is at present greatest. That is to say, the largest and significant increases in ROS frequency, duration, total precipitation and intensity are found in areas where there are at present very few, if any, ROS during the winter months.

Positive trends were exhibited by all ROS characteristics since 1991 using the CARRA dataset, but significant trends are confined to Nordaustlandet and Edgeøya, areas that are in closest proximity to sea ice presence during the winter. Sea ice extent around Svalbard has been declining (e.g., Onarheim et al., 2014) and it has been shown to be a key driver of strong warming trends across Spitsbergen (Isaksen et al., 2016, Isaksen et al., 2022) in recent decades. Wickström et al. (2020) found that local and regional sea ice extent drives seasonal variations in temperature and precipitation patterns across Svalbard, but the authors found less sensitivity of ROS to sea ice presence, as they found that ROS are primarily driven by the advection of warmer air masses from the southerly sector. Other studies of ROS events across the Yamal and Alaska have, on the other hand, noted below average sea ice concentration prior to events, suggesting a link between sea ice concentration and ROS (Forbes et al., 2016; Bartsch et al., 2023). While it has not been the objective of this study to quantify what role sea ice presence plays in the occurrence and observed trends in characteristics of ROS events, this could be an important topic to consider for future studies, given the rapid and ongoing decline of sea ice around Svalbard and across the polar regions, and its potential impact on atmospheric circulation and precipitation patterns.

Comparing the ROS characteristics of the CARRA dataset to those produced for the same period using the regional climate model driven with ERA5, it was found that the regional climate model projections provided by the HCLIM-ERA5 dataset reproduces the overall geographical variations in ROS frequency, duration, total precipitation, and intensity for the present/historical climate qualitatively well. However, the HCLIM-ERA5 datasets estimates slightly lower ROS frequency and duration compared to CARRA dataset over most of the archipelago. More conflicting results were found for the total precipitation and intensity, where HCLIM-ERA5 tended to estimate somewhat higher total precipitation across the western coast and southern parts of Nordaustlandet, but lower total precipitation across the rest of the archipelago. A comprehensive evaluation of the 2.5km-scale HCLIM-ERA5 simulations has recently been carried out (Landgren et al., 2025) and indicates that compared to CARRA, HCLIM tends to produce a slightly colder bias over land over most of Spitsbergen, but slightly warmer bias over eastern areas due to lack of snow cover over sea ice in ERA5 in the Barents sea region. This certainly could contribute to the differences we observed in the ROS characteristics between CARRA and HCLIM-ERA5, with underestimations in the characteristics by HCLIM over Spitsbergen but smaller differences over Nordaustlandet. Overall, the comparison of ROS climatology for the historical period demonstrates that the future projections of ROS characteristics should produce reliable climatologies. An additional source for the discrepancy in absolute values of the characteristics for the present



climate (2000-2020) could be due to the uncertainty in temperature threshold for partitioning rain and snow used in the different datasets. The temperature threshold for the CARRA dataset was determined via calibration against ground observations, and different datasets have been shown to require different temperature thresholds for detecting ROS (Vickers et al., 2024) whereas a calibration has not been done for the HCLIM-ERA5 simulations; therefore, applying the CARRA threshold to the HCLIM-ERA5 dataset cannot be expected to reproduce identical results.

Our analyses based on CARRA indicate that there have been significant and positive trends in ROS frequency since 1991 during October, November, February and May, and that the geographical variations in these trends are not the same in these months. While for the late autumn/early winter ROS the greatest trends have occurred over Nordaustlandet and eastern areas of Spitsbergen, in mid-winter (February) the trends in ROS frequency have been strongest across western and southern parts of Spitsbergen.

#### **4.2. Future projections of ROS characteristics**

In the two future periods examined in the HCLIM2.5-MPI simulation, areas that have exhibited increasing trends in the present climate, were projected to experience an increase in ROS frequency in October, November and May, but a decrease is projected along the western and southern coast of Spitsbergen. In contrast, HCLIM-MPI projected an increase in ROS in January and February over these same areas. The projected decreases in ROS frequency across western areas close to the coast could be attributed to a later onset and earlier disappearance of the snow season and thus a shorter period for rain to fall on snow. This scenario is also supported by the results published in a recent report by Landgren et al. (2025) that show that considerable decreases in the fraction of spring and autumn precipitation falling as snow are projected in the future scenario along the west and southern areas compared to the present day. While in the present climate there are almost no ROS events anywhere across the archipelago during March and April (Vickers et al., 2024), the HCLIM-MPI climate projections indicate that, by 2050-2070 April could experience considerable increases in mean number of ROS events. In terms of potential for ground ice formation, April is at present the month with typically greatest snow depths, and ROS events occurring during April may not contribute significantly to formation of ground ice as thicker snowpacks will typically absorb rain before it reaches the snow-ground interface (Peeters et al., 2019). Moreover, if the onset of spring snowmelt also occurs earlier in the future, then many of the projected April ROS events may correspond to rain falling on an already isothermal snowpack, which would unlikely result in ground ice but rather increased surface runoff, with knock-on implications for fjord and marine ecosystems. However, since there were projected to be similar increases in ROS events across large parts of the archipelago during late autumn/early winter, the November ROS events may result in early formation of ground ice, thereby creating the potentially difficult foraging conditions for herbivores such as reindeer that persists throughout the winter. On the other hand, a later onset of snow and thinner early winter snowpack, coupled with more frequent and intense ROS could lead to complete ablation of the snow cover, providing greater access to forage. The future situation of ground ice formation due to ROS and its associated impacts on ecosystems is therefore challenging to foresee based on atmospheric parameters alone.

398 We have focused on interpreting the potential impacts of the changes in ROS characteristics projected by HCLIM-MPI due to  
 399 its higher resolution offering better representation of the microphysical processes responsible for precipitation and extremes.  
 400 However, the uncertainty in these projected changes arising from the use of just one climate model must be considered when  
 401 drawing conclusions about future changes to ROS. While km-scale climate projections can reduce uncertainty by improving  
 402 the model representation of key physical processes, their computational cost prohibits the development of a model ensemble  
 403 to address uncertainty in downscaled projections. To partially address this, we analysed two additional HCLIM projections at  
 404 the coarser resolution of 11km that downscaled two other CMIP6 climate projections for the SSP3-7.0 scenario which is a  
 405 lower emission scenario than the SSP5-8.5 used in the km-scale simulations presented in this study (see Supplementary  
 406 material). These two coarser resolution HCLIM projections downscaled the CNRM-ESM2-1 and NorESM2-MM simulations  
 407 that were chosen using a storylines approach to address model uncertainty in the CMIP6 ensemble (Levine *et al.* 2024).  
 408 Our analysis of the coarser resolution HCLIM11-CNRM (Fig.S2) and HCLIM11-NorESM (Fig.S5) projections indicate that  
 409 there are areas with a large degree of uncertainty associated with the magnitude and polarity of the projected changes. This  
 410 uncertainty is demonstrated clearly by the HCLIM11-CNRM projections in Fig.S2 which projected decreases in all ROS  
 411 characteristics over most parts of Spitsbergen, and especially considerable reductions in ROS intensity and total precipitation  
 412 along the east coast of Spitsbergen for both future periods. These changes are opposite to those of the HCLIM-MPI and  
 413 HCLIM11-NorESM datasets which projected increases over most of the archipelago, but with different magnitudes of change.  
 414 This highlights the value in analysing projections with different physical storylines of future warming and addresses the range  
 415 of uncertainty in the future ROS climatology in Svalbard and moreover demonstrates the potential scope of change which the  
 416 ROS characteristics could fall within. These areas with greatest uncertainty, and hence least confidence are shown in grey in  
 417 Figure S8 and correspond to the areas where there was a lack of agreement in the sign of change between the three models. It  
 418 may be recognised that these are typically areas where ROS occur very infrequently in the present climate (Fig. 2), including  
 419 the high elevation areas in the northwest of Spitsbergen and Nordaustlandet, and inland and eastern parts of Spitsbergen. There  
 420 were nevertheless areas where we can have greater confidence in the projected changes, as shown by the areas where there  
 421 was agreement across the three GCMs in parts of northern Spitsbergen and the northern coastal areas of Nordaustlandet for all  
 422 four ROS characteristics. Moreover, it can be seen that in the 2050-2070 period, an increase in ROS frequency over northern  
 423 and eastern parts of Spitsbergen and Nordaustlandet carries more certainty, as shown by the agreement across all GCMs.  
 424 Recent studies have analysed circulation-specific precipitation patterns in the present and future climate in Svalbard (Dobler  
 425 et al., 2020) and find only small changes in the projected frequency of different weather types in the future climate, but  
 426 nevertheless relatively large increases in precipitation. The authors found that the greatest changes in precipitation are projected  
 427 to take place in the north and parts of the northeast of the archipelago, which was linked to higher precipitable water in the  
 428 atmosphere as a result of reduced sea ice extent and greater evaporation. These areas also correspond to where our analysis  
 429 found agreement in all three GCMs, with respect to increases in all ROS characteristics in the 2050-2070 period. On the other  
 430 hand, all three GCMs analysed in this study projected an overall reduction in ROS duration, total precipitation and intensity in  
 431 western parts of Spitsbergen which is unlikely explained by the same processes, or a reduced snow season length and could be

linked to changes in circulation patterns. While addressing the specific drivers of the observed patterns of change in ROS characteristics across the three climate models is outside the scope of the present study, further work could target determining the relative contributions of changes in sea ice concentration vs. remote (advected) moisture sources as drivers of the projected spatial variability of changes in ROS characteristics for a range of climate projections. Lastly, the high elevation parts of the archipelago that exhibit greatest relative change in ROS characteristics in the HCLIM-MPI dataset have earlier been shown to be the same areas with greatest projected decrease in average winter snow depths (Isaksen et al., 2017), primarily the glaciated areas north and northeast of Svalbard. Sobota et al. (2020) studied the impact of ROS events over small glaciers in northwestern Spitsbergen and found an increase over the period 1976-2018 resulting in more ice layers, noting that ROS intensity in particular controlled ice layer thickness. Other studies of ROS impacts over glaciers have used snow model simulations or in-situ observations and shown that ROS events may increase the wintertime glacier mass balance as percolated water refreezes in the snowpack (e.g., van Pelt et al., 2016; Łupikasza et al., 2019), while a recent review of winter warm spells and heat waves highlights potential alteration of the glacier thermal regime when snow falls at relatively warm temperatures (Spolaor et al., 2025). Indeed, a recent study combined a set of ice core observations together with modelling of glacier stratigraphy and identified a transition in the thermal regime and stratigraphy of Austfonna in the northeast of Svalbard since 2013, from cold to temperate firn above the ice-firn interface (Innanen et al., 2025). In areas with large snow accumulation, multiple ROS events throughout the winter contribute to ice layers forming within the snowpack, which influences how rainwater from subsequent ROS events percolates through the snowpack, with knock-on impacts for runoff generation. Overall, the snowpack characteristics may be impacted by the significant increases in ROS that are projected to take place over Svalbard's glaciated areas within the next 50 years, although there nevertheless remains a lot of uncertainty in the polarity of change in some areas. While these areas may not be significant for land-based herbivores, increased melt and/or runoff from glaciers could have indirect ecological impacts by contributing with freshwater input to coastal or fjord environments, with subsequent impacts on fjord biogeochemistry and ecosystems (e.g, Vonnahme et al., 2023).

#### 4.3 Limitations of the study

This study has utilized only one regional climate model to downscale one global climate model covering the high emissions SSP5-8.5 scenario. While this allows for an improved simulation of precipitation over smaller spatial scales which is crucial for mountainous and glaciated areas such as Svalbard, the use of only one RCM is a major limitation in capturing model parameterisation uncertainty and internal climate variability. Moreover, there remains a large degree of uncertainty in the magnitude and patterns of precipitation changes simulated by GCMs at local scales, limiting their use in risk assessments. These uncertainties have been in part demonstrated by our analysis of two additional 11km-scale climate projections, which showed that some areas of the archipelago that currently experience relatively few ROS events in the winter, carry greatest uncertainty, as exhibited by the opposite signs of change projected by the HCLIM11-CNRM and HCLIM11-NorESM projections (Fig. S2, S5). On the other hand, the areas which carried greater certainty in the projected sign of change were not constant across the two future periods analysed. The lack of agreement across the models across these areas also calls for a

more comprehensive analysis of the drivers of change, examining the relative importance of changes in snow season, and remote vs. local moisture sources. Future work should exploit an ensemble of models to produce a more robust projection of changes in ROS characteristics to identify similarities or discrepancies in the patterns of change across different models. It should also be emphasized that while the SSP5-8.5 scenario, represented by the km-scale HCLIM projections is a more extreme scenario based on current energy trends and socio-economic circumstances, it is nonetheless a plausible scenario and provides an upper bound on the range of possibilities and highlights the full range of risks for policymakers, so that they can understand what happens if mitigation measures fail.

Our approach utilizes daily values of meteorological (mean air temperature, precipitation) and surface (snow depth water equivalent) variables to detect days with rain-on-snow. These variables are commonly available across different reanalysis and climate model datasets which therefore makes the approach reproducible for other regions of the world where the impacts of ROS are consequential. However, a weakness in this approach is that the rain-snow transition is not properly represented. RCMs at km-scales offer a physics-based approach as the precipitation processes are represented exclusively by the microphysical scheme which separates precipitation into liquid and solid forms based on physics. This contrasts with coarser RCMs which must use both a microphysics scheme and a cumulus scheme, the latter of which cannot separate precipitation into liquid and solid form explicitly, thus necessitating the use of temperature-based approach. We have attempted to address this aspect by comparing the climatologies of each ROS characteristic for the 2000-2020 period using the HCLIM-ERA5 dataset, using temperature thresholds ranging from  $-0.5^{\circ}\text{C}$  to  $0.5^{\circ}\text{C}$ , and when using the *prrain* variable, which gives 3-hourly estimates of the precipitation falling as rain (Figure A2). While there was better agreement between the *prrain*-based detection of ROS, and the temperature-thresholded approach using  $T=-0.5^{\circ}\text{C}$  for the ROS frequency and duration for the archipelago as a whole, this temperature threshold produced much greater estimates of ROS total precipitation and intensity, especially in the western and southern parts of the archipelago. This is most likely an effect of taking a daily precipitation sum on days where the daily mean temperature exceeded this threshold. Whereas the *prrain*-based detection gives the total sum of rain on days with snow cover, the temperature threshold-based approach would most likely overestimate the total precipitation falling as rain, especially if there are wide variations in the daily temperatures. However, when examining the future changes of ROS in terms of the spatial variations, calculated using *prrain* (Fig. A3 to A5) the overall conclusions remain unchanged. Moreover, it should be highlighted that the temperature-based approach for partitioning rain and snow is nevertheless valid and necessary in cases where datasets have much coarser spatial resolution (eg  $>12$  km) or temporal resolution and remains the only approach using ground observations where precipitation phase data are unavailable.

Hydrological modelling should also be considered, given that our analysis suggests a shift towards a large increase in ROS frequency in April. While April is a present typically a month with greatest snow depths and sea ice concentration around Svalbard, in a future climate April may be important for the onset of spring snowmelt, thus a large increase in ROS could also increase the potential for flooding impacts through enhanced runoff due to the combination of rain and rain-amplified snowmelt. There is also an uncertainty in how runoff may be affected by the presence of multiple ice layers within a snowpack caused by increased ROS frequency in areas with large snow accumulations. These impacts could be addressed in greater

499 detail to follow up the initial results presented here. Moreover, the potential link between sea ice concentration and ROS events  
500 should be more carefully assessed and quantified, given the impact of continued rapid climate warming in the polar regions on  
501 sea ice cover.

## 502 **5 Conclusion**

503 This study has examined five specific characteristics of rain-on-snow events across Svalbard in the present climate using the  
504 CARRA reanalysis dataset, and in the future climate using high resolution 2.5 km-scale simulations from the HCLIM regional  
505 climate model. ROS frequency, duration, total precipitation, intensity and seasonality were quantified. We found significant  
506 and positive trends in all characteristics, but the significant trends were confined mainly to areas around the low-lying parts of  
507 Nordaustlandet and areas in the east of the archipelago, while southern and western areas that typically exhibit greatest values  
508 in all characteristics, were not found to exhibit significant trends in duration, total precipitation or intensity since 1991. Using  
509 the same approach to quantify ROS, the HCLIM dataset driven by ERA5 input showed good agreement in the geographic  
510 variability of all characteristics, though there were small differences in the absolute values. The HCLIM-MPI simulations for  
511 2030 to 2070 project the greatest changes relative to present day conditions for all ROS characteristics in the mountainous  
512 and glaciated areas to the north and northeast of the archipelago, while low lying western coastal areas are projected to decrease  
513 in all characteristics.

514 We have attempted to address the uncertainty associated with using only one high resolution RCM and one GCM by analysing  
515 two other HCLIM projections at the coarser resolution of 11km for the SSP3-7.0 scenario. Comparison of the km-scale SSP5-  
516 8.5 HCLIM-MPI projections at 2.5km with these two coarser, SSP3-7.0. HCLIM projections show that there are large areas  
517 of the archipelago where the change in ROS is uncertain, especially with regard to the magnitude and sign of change in the  
518 ROS characteristics and demonstrated by the lack of agreement across the three GCMs analysed. However, these findings also  
519 highlight the value in analysing projections from three GCMs that present different storylines of warming, specifically that the  
520 range of uncertainty in future ROS climatology is addressed, as well as being able to identify areas where the changes are more  
521 certain.

522 Changes in the length of the snow covered season when ROS can occur may affect the changes in frequency of ROS, but more  
523 precipitable water in the atmosphere has been shown in similar studies to be a likely driver of increases in precipitation in  
524 particular over northern and northeastern areas, where declining sea ice leads to greater surface evaporation. Lastly, our  
525 analysis indicates that ROS have been increasing most in October, November, February and May, but in contrasting areas of  
526 the archipelago. While ROS have increased most in the eastern and northeastern parts of Svalbard in October and November,  
527 areas that are typically sensitive to sea ice concentration, it is primarily the western and southern parts of Spitsbergen that have  
528 experienced significant increases in ROS frequency in February. The projections of Svalbard's future climate shows that there  
529 could be an increase in ROS events across all months under a high emissions scenario, but substantial increases are also  
530 projected to occur in January and April for the 2050-2070 period, months which currently experience very few, if any, ROS

531 events. This shift in ROS timing may have a cascade of impacts for both terrestrial and marine ecosystems that are dependent  
532 on snow and snowmelt.

### 533 **Data Availability**

534 The CARRA dataset is publicly available and can be downloaded from the Copernicus Climate Data Store (CDS). The HCLIM  
535 2.5 km regional climate simulations are available from <https://thredds.met.no/thredds/catalog/pcch-arctic/catalog.html> Until  
536 publicly available via ESGF, the 11 km HCLIM downscaled CNRM and NorESM datasets are available upon request to  
537 [cordex@met.no](mailto:cordex@met.no).

### 538 **Author Contribution**

539 HV and PM designed the study, OL prepared and made available the climate simulations, HV carried out the data analysis and  
540 prepared the manuscript with contributions from all co-authors.

### 541 **Competing Interests**

542 The authors declare that they have no conflict of interest.

### 543 **Acknowledgements**

544 This research was funded by Svalbard's Environmental Protection fund (grant 24/20) and the Framsenter research cooperation  
545 (incentive project CHORUS), and the Norwegian Research Council, project "PCCH-Arctic", under grant ID 320769. The  
546 climate simulations were carried out on the Norwegian Research Infrastructure Services (NRIS) high-performance computing  
547 facility "Betzy", operated by Sigma2, under project number NN9875K.

548 We acknowledge the support of PolarRES (grant no. 101003590), a project of the European Union's Horizon 2020 research  
549 and innovation programme. Storage and computing resources necessary to conduct the analysis were provided by Sigma2 –  
550 the national infrastructure for high-performance computing and data storage in Norway (project nos. NS8002K and  
551 NN8002K).

### 552 **References**

553 Bartsch, A., Bergstedt, H., Pointner, G., Muri, X., Rautiainen, K., Leppänen, L., Joly, K., Sokolov, A., Orekhov, P., Ehrich,  
554 D., and Soininen, E. M.: Towards long-term records of rain-on-snow events across the Arctic from satellite data, The  
555 Cryosphere, 17, 889–915, <https://doi.org/10.5194/tc-17-889-2023>, 2023.

557 Belušić, D., de Vries, H., Dobler, A., Landgren, O., Lind, P., Lindstedt, D., Pedersen, R. A., Sánchez-Perrino, J. C., Toivonen,  
 558 E., van Uft, B., Wang, F., Andrae, U., Batrak, Y., Kjellström, E., Lenderink, G., Nikulin, G., Pietikäinen, J.-P., Rodríguez-  
 559 Camino, E., Samuelsson, P., van Meijgaard, E., and Wu, M.: HCLIM38: a flexible regional climate model applicable for  
 560 different climate zones from coarse to convection-permitting scales, *Geosci. Model Dev.*, 13, 1311–1333,  
 561 <https://doi.org/10.5194/gmd-13-1311-2020>, 2020.

563 Day, J. J., Bamber, J. L., Valdes, P. J., and Kohler, J.: The impact of a seasonally ice free Arctic Ocean on the temperature,  
 564 precipitation and surface mass balance of Svalbard, *The Cryosphere*, 6, 35–50, <https://doi.org/10.5194/tc-6-35-2012>, 2012.

566 Dobler, A., Lutz, J., Landgren, O., & Haugen, J. E. (2020). Circulation Specific Precipitation Patterns over Svalbard and  
 567 Projected Future Changes. *Atmosphere*, 11(12), 1378. <https://doi.org/10.3390/atmos11121378>

569 Forbes, B. C., Kumpula, T., Meschtyb, N., Laptander, R., Macias-Fauria, M., Zetterberg, P., Verdonen, M., Skarin, A., Kim,  
 570 K. Y., Boisvert, L. N., Stroeve, J. C., & Bartsch, A.: Sea ice, rain-on-snow and tundra reindeer nomadism in Arctic Russia,  
 571 *Biology Letters*, 12(11), 20160466. <https://doi.org/10.1098/rsbl.2016.0466>, 2016.

573 Førland E. J., Benestad, R.E., Hanssen-Bauer, I., Haugen, J.E. and Skaugen, T.E.: Temperature and Precipitation Development  
 574 at Svalbard 1900–2100, *Adv. Meteor.*, 2011, 1–14, doi:10.1155/2011/893790, 2011.

576 Gutjahr, O., Putrasahan, D., Lohmann, K., Jungclaus, J. H., von Storch, J.-S., Brüggemann, N., Haak, H., and Stössel, A.: Max  
 577 Planck Institute Earth System Model (MPI-ESM1.2) for the High-Resolution Model Intercomparison Project (HighResMIP),  
 578 *Geosci. Model Dev.*, 12, 3241–3281, <https://doi.org/10.5194/gmd-12-3241-2019>, 2019.

580 Hansen, B. B., Isaksen, K., Benestad, R. E., Kohler, J., Pedersen, Å. Ø., Loe, L. E., Coulson, S. J., Larsen, J. O., & Varpe, Ø.:  
 581 Warmer and wetter winters: Characteristics and implications of an extreme weather event in the High Arctic. *Environmental*  
 582 *Research Letters*, 9(11), 114021, <https://doi.org/10.1088/1748-9326/9/11/114021>, 2014.

584 Hanssen-Bauer, I., Førland, E.J., Hisdal, H., Mayer, S., Sandø, A.B. and Sorteberg, A.: Climate in Svalbard 2100. NCCS Rep.  
 585 1/2019, 205 pp., <https://www.miljodirektoratet.no/globalassets/publikasjoner/M1242/M1242.pdf>, 2019

586 Hopwood et al., 2020 Hopwood, M. J., Carroll, D., Dunse, T., Hodson, A., Holding, J. M., Iriarte, J. L., Ribeiro, S., Achterberg,  
 587 E. P., Cantoni, C., Carlson, D. F., Chierici, M., Clarke, J. S., Cozzi, S., Fransson, A., Juul-Pedersen, T., Winding, M. H. S.,  
 588 and Meire, L.: Review article: How does glacier discharge affect marine biogeochemistry and primary production in the  
 589 Arctic?, *The Cryosphere*, 14, 1347–1383, <https://doi.org/10.5194/tc-14-1347-2020>, 2020.

591 Hersbach, H., Bell, B., Berrisford, P., Hirahara, S., Horányi, A., Muñoz-Sabater, J., Nicolas, J., Peubey, C., Radu, R., Schepers,  
 592 D., Simmons, A., Soci, C., Abdalla, S., Abellan, X., Balsamo, G., Bechtold, P., Biavati, G., Bidlot, J., Bonavita, M., De Chiara,  
 593 G., Dahlgren, P., Dee, D., Diamantakis, M., Dragani, R., Flemming, J., Forbes, R., Fuentes, M., Geer, A., Haimberger, L.,  
 594 Healy, S., Hogan, R. J., Hólm, E., Janisková, M., Keeley, S., Laloyaux, P., Lopez, P., Lupu, C., Radnoti, G., de Rosnay, P.,  
 595 Rozum, I., Vamborg, F., Villaume, S. & Thépaut, J. N.: The ERA5 global reanalysis, *Quarterly Journal of the Royal*  
 596 *Meteorological Society*, 146(730), 1999-2049. <https://doi.org/10.1002/qj.3803>, 2020

597

598 Innanen, S., Hock, R., Schmidt, L.S., Schuler, T.V., Covi, F. and Moholdt, G.: Witnessing the transition from cold to temperate  
 599 firn on Austfonna ice cap, Svalbard through observations and model simulations, *J. Glaciology*, 71:e101,  
 600 doi:10.1017/jog.2025.10072, 2025

601

602 Isaksen, K., Nordli, Ø., Førland, E.J., Łupikasza, E., Eastwood, S. and Niedźwiedź, T.: Recent warming on Spitsbergen—  
 603 Influence of atmospheric circulation and sea ice cover, *J. Geophys. Res. Atmos.*, 121, 11,913–11,931,  
 604 doi:10.1002/2016JD025606, 2016.

605

606 Isaksen, K., Førland, E.J., Dobler, A., Benestad, R., Haugen, J.E. and Mezghani, A.: Klimascenarioer for Longyearbyen-  
 607 området, Svalbard, MET Norway Report 14/2017, 2017.

608

609 Isaksen et al., 2022 Exceptional warming over the Barents Sea <https://www.nature.com/articles/s41598-022-13568-5>

610 Isaksen, K., Nordli, Ø., Ivanov, B. *et al.*: Exceptional warming over the Barents area. *Sci. Rep.*, 12, 9371,  
 611 <https://doi.org/10.1038/s41598-022-13568-5>, 2022.

612

613 Køltzow, M., Casati, B., Bazile, E., Haiden, T. and Valkonen, T.: An NWP model intercomparison of surface weather  
 614 parameters in the European Arctic during the year of polar prediction special observing period Northern Hemisphere 1,  
 615 *Weather Forecast.* 34, 959–983. doi:10.1175/WAF-D-19-0003, 2019.

616

617 Køltzow, M., Schyberg, H., Støylen, E., and Yang, X.: Value of the Copernicus Arctic Regional Reanalysis (CARRA) in  
 618 representing near-surface temperature and wind speed in the north-east European Arctic, *Polar Res.* 41, 8002.  
 619 doi:10.33265/polar.v41.8002, 2022.

620

621 Landgren, O., Lutz, J., Dobler, A., and Isaksen, K.: Multi-decadal convection-permitting climate simulation over Svalbard and  
 622 its benefit for assessing the future of cultural heritage sites, *EMS Annual Meeting 2022*, Bonn, Germany, 5–9 Sep 2022, EMS,  
 623 2022-556, <https://doi.org/10.5194/ems2022-556>, 2022.



624

625 Landgren, O., Lutz, J., Isaksen, K.: 2.5 km future climate projections for Svalbard under the high emission scenario SSP5-8.5,  
626 MET Report 1/2025, ISSN 2387-4201, 2025.

627

628 Levine, X. J., Williams, R. S., Marshall, G., Orr, A., Seland Graff, L., Handorf, D., Karpechko, A., Köhler, R., Wijngaard, R.  
629 R., Johnston, N., Lee, H., Nieradzik, L., and Mooney, P. A.: Storylines of summer Arctic climate change constrained by  
630 Barents–Kara seas and Arctic tropospheric warming for climate risk assessment, *Earth Syst. Dynam.*, 15, 1161–1177,  
631 <https://doi.org/10.5194/esd-15-1161-2024>, 2024

632

633 Łupikasza, E.B., Ignatiuk, D., Grabiec, M., Cielecka-Nowak, K., Laska, M., Jania, J., Luks, B., Uszczyk, A. and Budzik, T.:  
634 The Role of Winter Rain in the Glacial System on Svalbard, *Water*, 11(2):334. <https://doi.org/10.3390/w11020334>, 2019.

635

636 Mooney P.A., Sobolowski, S. and Lee, H.: Designing and evaluating regional climate simulations for high latitude land use  
637 land cover change studies, *Tellus Dyn. Meteorol. Oceanogr.* 72 1–17, 2020.

638

639 Mooney, P. A., and Li, L.: Near future changes to rain-on-snow events in Norway, *Environ. Res. Lett.* 16, 064039.  
640 doi:10.1088/1748-9326/abfdeb, 2021.

641

642 Onarheim, I.H., Smedsrud, L.H., Ingvaldsen, R.B. and Nilsen, F.: Loss of sea ice during winter north of Svalbard, *Tellus A:*  
643 *Dynamic Meteorology and Oceanography*, 66(1), <https://doi.org/10.3402/tellusa.v66.23933>, 2014.

644

645 Pedersen Å.Ø., Beumer, L.T., Aanes, R. and Hansen, B.B.: Sea or summit? Wild reindeer spatial responses to changing high-  
646 arctic winters, *Ecosphere*, 12(12):e03883. 101002/ecs2.3883, 2021.

647

648 Peeters, B., Pedersen, Å. Ø., Loe, L. E., Isaksen, K., Veiberg, V., Stien, A., Kohler, J., Gallet, J. C., Aanes, R., & Hansen, B.  
649 B.: Spatiotemporal patterns of rain-on-snow and basal ice in high Arctic Svalbard: Detection of a climate-cryosphere regime  
650 shift, *Environmental Research Letters*, 14(1), 015002, <https://doi.org/10.1088/1748-9326/aaefb3>, 2019.

651

652 Prein, A.F. et al.: A review on regional convection-permitting climate modeling: demonstrations, prospects, and challenges  
653 *Rev. Geophys.* 53(2), 323–361, doi: 10.1002/2014RG000475, 2015.

654

655 Schyberg, H., Yang, X., Køltzow, M. A. Ø., Amstrup, B., Bakketun, Å., Bazile, E., et al.: Arctic regional reanalysis on single  
656 levels from 1991 to present, Copernicus Climate Change Service, doi:10.24381/cds.713858f, 2020.

657  
658  
659  
660  
661  
662  
663  
664  
665  
666  
667  
668  
669  
670  
671  
672  
673  
674  
675  
676  
677  
678  
679  
680  
681  
682  
683  
684  
685  
686  
687

Screen, J. A. & Simmonds, I.: Increasing fall-winter energy loss from the Arctic Ocean and its role in Arctic temperature amplification. *Geophys. Res. Lett.* 37, L16707, 2010

Serreze, M., Gustafson, J., Barrett, A.P., Druckenmiller, M.L., Fox, S., Voveris, J., Stroeve, J., Sheffield, B., Forbes, B.C., Rasmus, S., Laptander, R., Brook, M., Brubaker, M., Temte, J., McCrystall, M.R. and Bartsch, A.: Arctic rain on snow events: bridging observations to understand environmental and livelihood impacts, *Environmental Research Letters*, 16(10), DOI 10.1088/1748-9326/ac269b, 2021.

Shepherd, T.G., Boyd, E., Calel, R.A. et al.: Storylines: an alternative approach to representing uncertainty in physical aspects of climate change, *Climatic Change*, 151, 555–571, <https://doi.org/10.1007/s10584-018-2317-9>, 2018.

Sobota, I., Weckwerth, P. and Grajewski, T.: Rain-On-Snow (ROS) events and their relations to snowpack and ice layer changes on small glaciers in Svalbard, the high Arctic, *Journal of Hydrology*, 590, 125279, <https://doi.org/10.1016/j.jhydrol.2020.125279>, 2020.

Spolaor, A., Salzano, R., Scoto, F., Barbaro, E., Luks, B., Laska, M., Sobota, I., Maetze, R., Malnes, E., Vickers, H., Larose, C., Dahlke, S. and Maturilli, M.: Understanding and analysing recurrent warm events in Svalbard: a comprehensive review on land cryosphere (AWARE), SESS report 2024 - The State of Environmental Science in Svalbard - an annual report, 212-226, Svalbard Integrated Arctic Earth Observing System, <https://doi.org/10.5281/zenodo.14425903>, 2025.

Van Pelt, W. J. J., Kohler, J., Liston, G.E., Hagen, J.O., Luks, B., Reijmer, C.H. and Pohjola, V.A.: Multidecadal climate and seasonal snow conditions in Svalbard, *J. Geophys. Res. Earth Surf.*, 121, 2100–2117, doi:[10.1002/2016JF003999](https://doi.org/10.1002/2016JF003999), 2016.

Vickers, H., Malnes, E., and Eckerstorfer, M.: A Synthetic Aperture Radar Based Method for Long Term Monitoring of Seasonal Snowmelt and Wintertime Rain-On-Snow Events in Svalbard, *Front. Earth Sci.*, 10, 868945, <https://doi.org/10.3389/feart.2022.868945>, 2022.

Vickers, H., Saloranta, T., Køltzow, M., van Pelt Ward J. J. and Malnes, E.: An analysis of winter rain-on-snow climatology in Svalbard, *Front. Earth Sci.*, 12, <https://doi.org/10.3389/feart.2024.1342731>, 2024.

688 Vonnahme, T.R., Nowak, A., Hopwood, M.J., Meire, L., Søgaaard, D.H., Krawczyk, D., Kalhagen, K. and Juul-Pedersen, T.:  
689 Impact of winter freshwater from tidewater glaciers on fjords in Svalbard and Greenland; A review, Progress in Oceanography,  
690 219, 103144, <https://doi.org/10.1016/j.pocean.2023.103144>, 2023.

691

692 Wang, F.: An introduction to the HARMONIE-Climate (HCLIM) regional climate modeling system. Zenodo.  
693 <https://doi.org/10.5281/zenodo.11424181>, 2024.

694

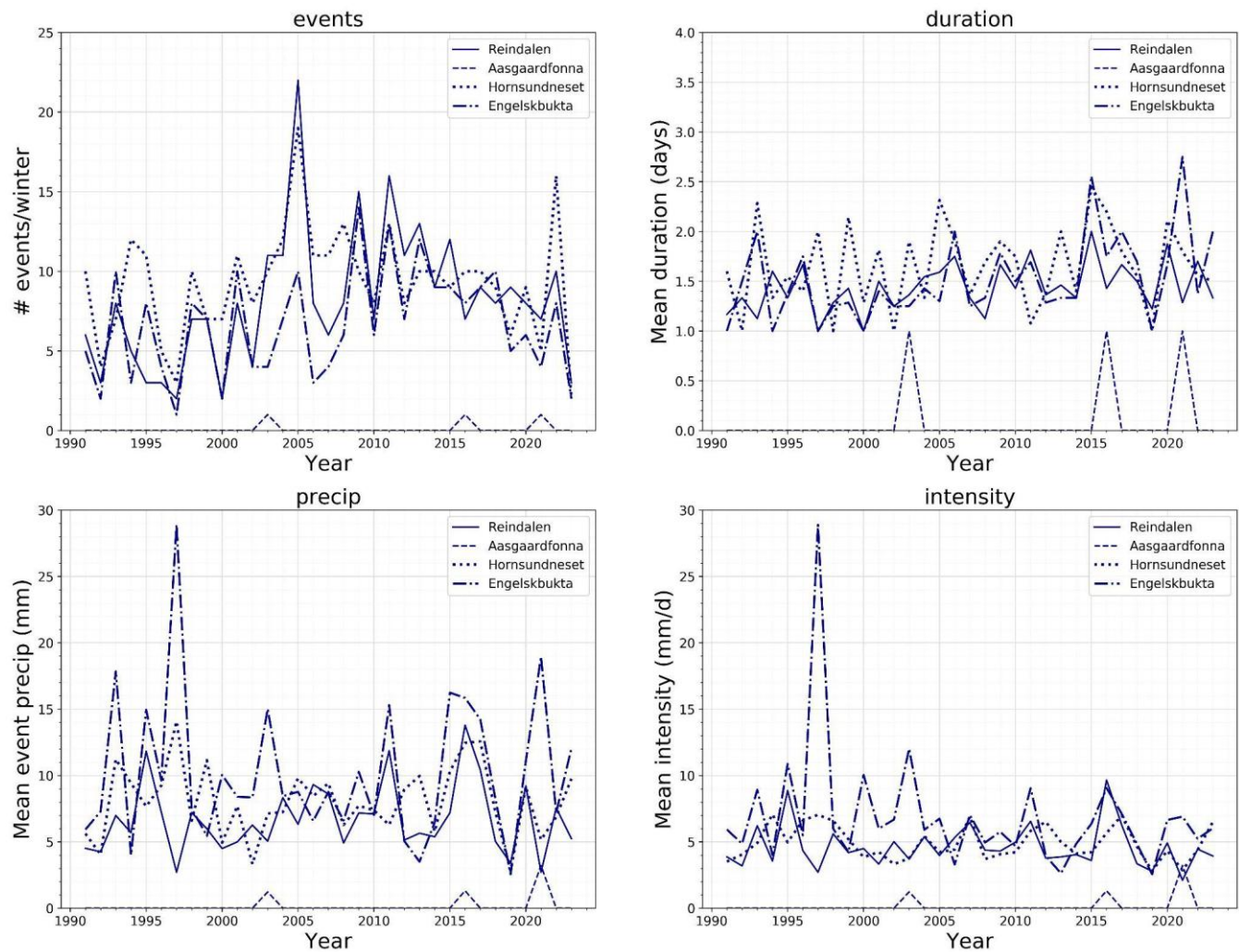
695 Wickström, S., Jonassen, M. O., Cassano, J. J., and Vihma, T.: Present temperature, precipitation, and rain-on-snow climate  
696 in Svalbard. Journal of Geophysical Research: Atmospheres, 125, <https://doi.org/10.1029/2019JD032155>, 2020.

697

698 Würzer, S., Jonas, T., Wever, N. and Lehning, M.: Influence of initial snowpack properties on runoff formation during rain-  
699 on-snow events. J. Hydrometeor., 17, 1801-1815, <https://doi.org/10.1175/JHM-D-15-0181>, 2016.

700

701 Zhang, R. et al. Understanding the cold season Arctic surface warming trend in recent decades. Geophys Res Lett. 48,  
702 e2021GL094878, 2021



705 **Figure A1. Time series of the ROS characteristics (number of events, mean duration, mean total precipitation and mean intensity)**  
706 **shown for four contrasting sites across Spitsbergen; Reindalen (77.98°N, 16.07°E), Åsgårdfonna (79.61°N, 16.61°E), Hornsundneset**  
707 **(76.88°N, 15.57°E) and Engelsbukta (78.84°N, 11.98°E). The coordinates correspond to one point within each area and are not**  
708 **exact coordinates for each site.**

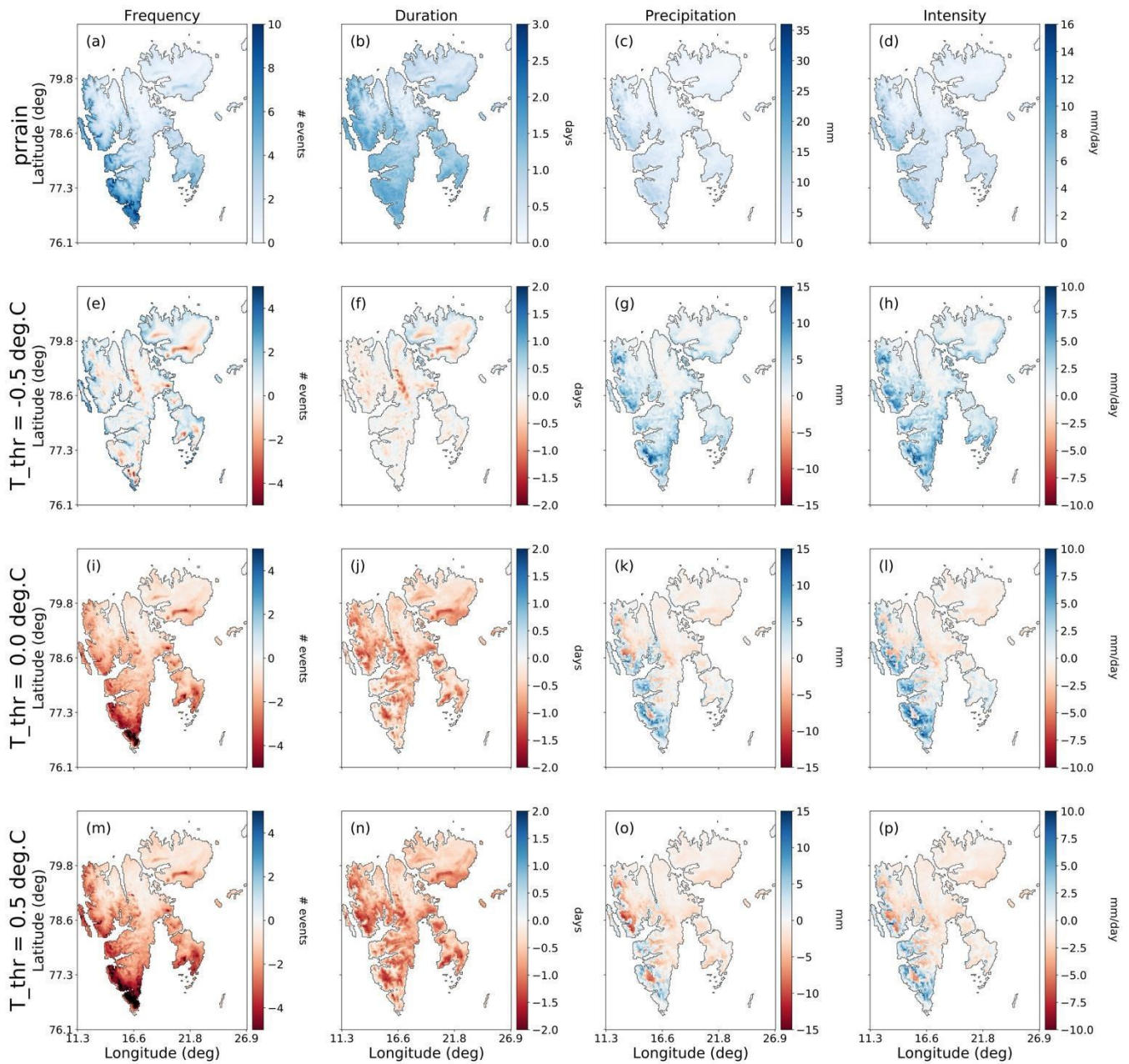


**Figure A2. Mean ROS characteristics for the historical period (2000-2020) produced using the HCLIM-ERA5 dataset using the accumulated rain variable (*prrain*) for detection, and the differences between the temperature-thresholded ( $t_{thr}$ ) approach using thresholds of  $-0.5^{\circ}\text{C}$ ,  $0.0^{\circ}\text{C}$  and  $0.5^{\circ}\text{C}$ . The difference is given as  $\text{ROS}(t_{thr})$  minus  $\text{ROS}(prrain)$  such that blue shades indicate areas where the temperature-threshold approach produced higher values than *prrain*, and red areas indicate areas where *prrain* produced higher values of the ROS variable compared to the temperature threshold detection.**



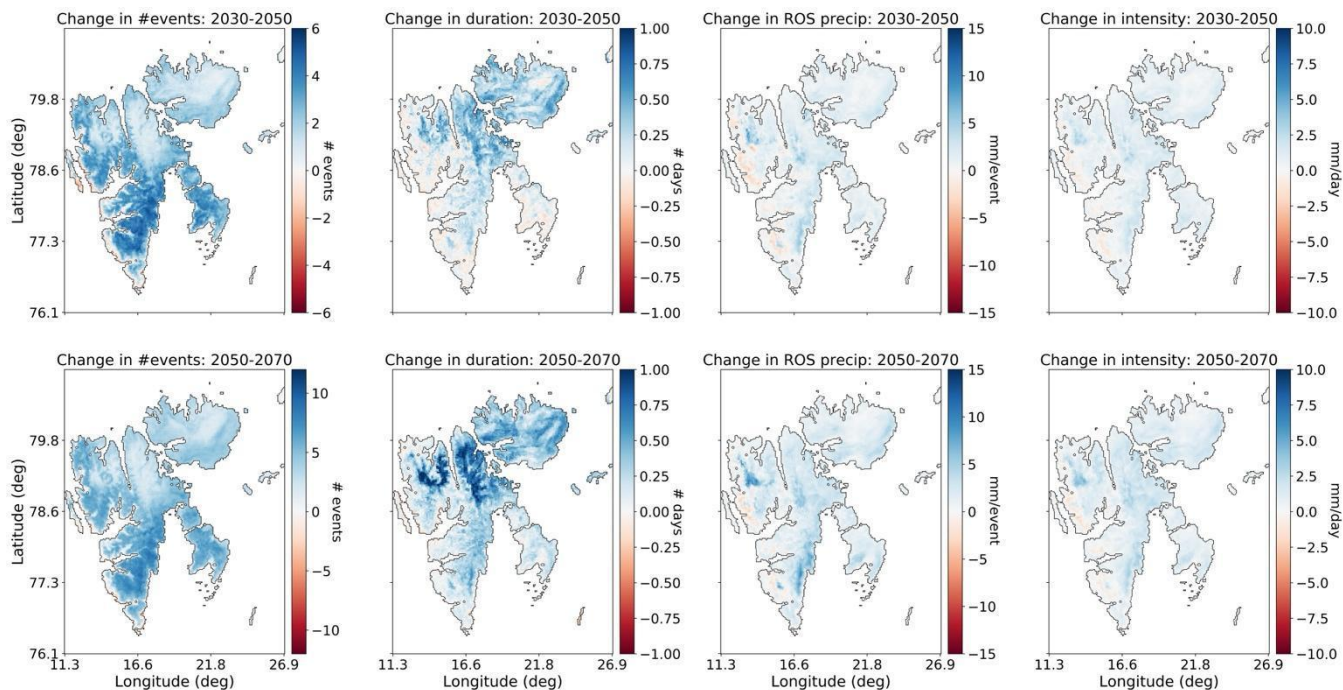


**Figure A3. Change in ROS frequency, duration, total precipitation, and mean intensity for 2030-2050 (upper row) and 2050-2070 (lower row) relative to the 2000-2020 averages, using the *prrain* variable to detect ROS.**

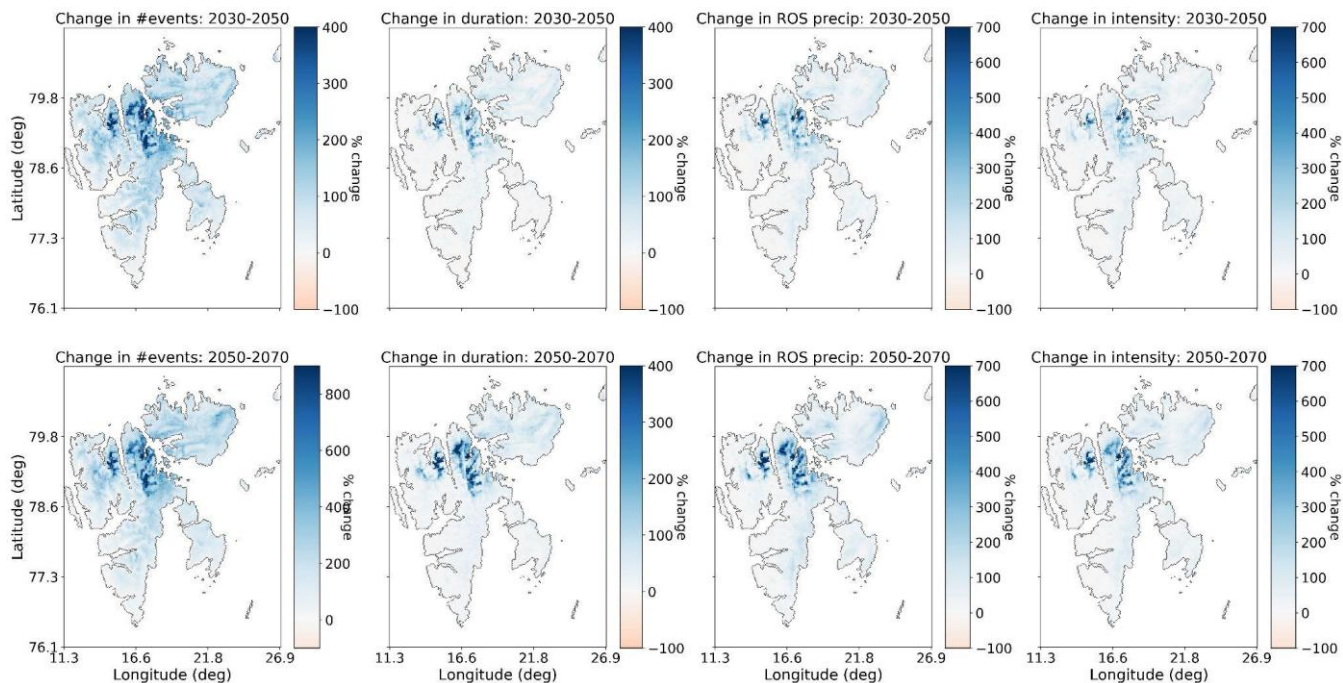


**Figure A4. As for Fig. A3 but with the changes expressed as a percentage of the 2000-2020 values.**

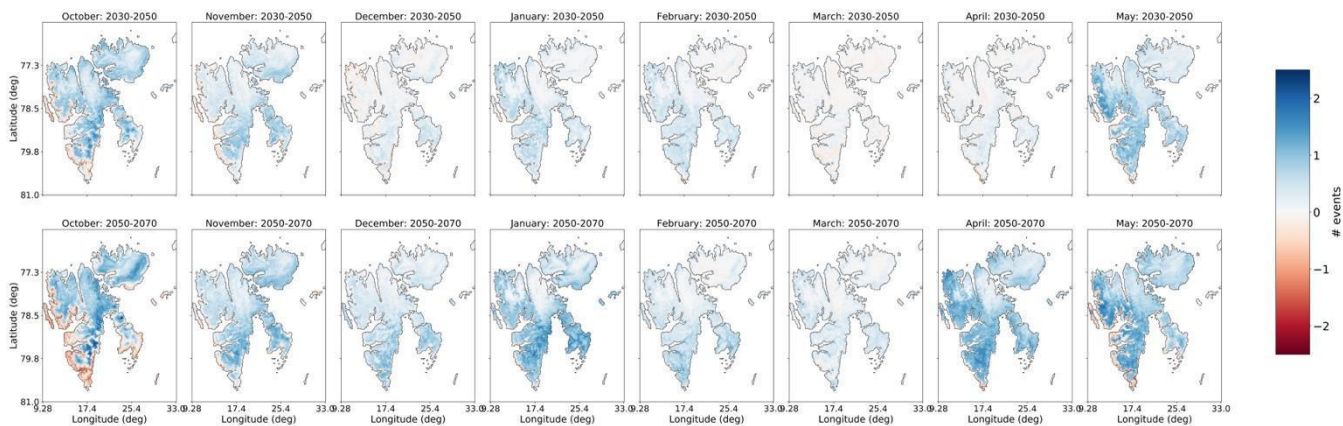


**Figure A5. Changes in ROS frequency by month from October to May for 2030-2050 (upper row) and 2050-2070 relative to the reference period 2000-2020, when ROS were detected using the *prrain* variable.**